JMEPEG (2018) 27:6701–6708
https://doi.org/10.1007/s11665-018-3760-5

1059-9495/$19.00

The Improved Thermal Conductivity of a Potting Material for High-Power Fast Warm-Up Cathodes

Xiaodong Zhang, Junjie Hao, Zhimeng Guo, Zhenhui Ji, Ji Luo, Cunguang Chen, Fang Yang, and Alex A. Volinsky

(Submitted December 18, 2017; in revised form August 29, 2018; published online November 27, 2018)

With higher power, frequency and longer life of microwave tubes, cathode heater assembly is being modified to enhance the warm-up performance and reliability, which are governed by ceramics thermal conductivity, electrical resistivity and shrinkage. In present work, a potting material with a high thermal conductivity of 22.14 W/(m K) and low linear shrinkage of 5.5% was prepared using two kinds of alumina powders with different size and morphology. Aqueous slurries were produced for centrifugal casting. The highest solid loading slurries with 70 vol.% were obtained. Green body with relative density above 70% was easily made from slurries using centrifugal casting. Relative sintered density reached 86.75% maximum without any sintering aids. Rheological behavior of slurries, potting microstructure, sintering shrinkage and thermal conductivity were analyzed. Continuous particle distribution, series and parallel models were used to guide the powders proportion and explain the thermal conductivity. The potting material thermal conductivity experimental data agreed with the series and parallel models when the weight parameter ξ was between 0.3 and 0.5.

Keywords centrifugal casting, fast warm-up cathodes, high solid-loaded slurries, high thermal conductivity, low liner shrinkage

1. Introduction

Fast warm-up traveling-wave tubes are widely used in military and aerospace applications, including electronic warfare, missile seekers and conventional radars with the cathode reaching its maximum electron emission in several seconds (Ref 1). The dielectric potting material (Fig. 1(4)) is used to package a coiled filament wire (Fig. 1(3)) and a support cylinder (Fig. 1(2)), which collectively form the heater assembly. Generally, the cathode (Fig. 1(1)) brazed to the support cylinder is indirectly heated to produce thermionically emitted electrons.

Voltage is applied to the filament in 10^{-8} Torr vacuum to raise its temperature to at least 1050-1200 °C in a few seconds to provide the thermal energy to promote thermal electron emission from the cathode. The heater assembly geometry is shown in Fig. 1. The thermal conductivity and linear shrinkage of the potting material directly determine the warm-up properties, lifetime and reliability of traveling-wave tubes (Ref 1). The linear shrinkage of the potting material controls the sintering shrinkage and the thermal expansion.

The most desired qualities of such potting materials are maximum thermal conductivity, high electrical resistivity, the proper coefficient of thermal expansion (CTE) and minimum shrinkage during drying/firing without any undesirable reactivity toward surrounding metals (Ref 2). Due to the small dimensions of the heater assembly (3-15 mm), the shrinkage of 5-15% is much larger during sintering (Ref 2-5), so only the shrinkage during sintering of the potting materials is discussed in the present work. Alpha-alumina (α-Al_2O_3) is one of the widely used potting materials because of its abundance and unique mechanical, electrical and thermal properties (Ref 2, 3). There is currently no alternative potting material, which can completely substitute alumina. Alternative potting materials must meet fast warm-up time requirement, conduct heat faster and withstand much higher thermal stresses than standard alumina (Ref 1, 3).

Intensive research has been carried out toward obtaining a potting material with higher thermal conductivity and density. Various formulations and mixes of different grit size doped alumina and modifications of potting and sintering processes are used to reduce shrinkage and crack formation. Thus, the potting mixtures are denser and capable of withstanding fast heating (Ref 1-5).

Orlowska (Ref 1) demonstrated alumina-based potting ceramics, which would conduct heat faster. Wolverton et al. (Ref 5) demonstrated 97% alumina composition with thermal diffusivity of 1.12 mm^2/s at room temperature. Swartzentruber et al. (Ref 3) showed that Al_2O_3/AlN/CaO had 3 W/(m K) thermal conductivity. Kalyan et al. (Ref 2) reported that 1 wt.% CaO-doped Al_2O_3 samples had a higher thermal conductivity of 19.44 W/(m K) at 200 °C with low 2.89% shrinkage and decreased electrical resistivity.

Not enough liquid phase would concomitantly result in ceramics shrinkage with delamination and tiny cracks between potting and the support cylinder during sintering. However, excess liquid solution decreases the electrical resistivity of potting mixtures (Ref 2), which could reduce the reliability of the heater assembly.

With the quest for microwave tubes with higher power and/or higher frequencies, longer life or combinations of these, cathode

Xiaodong Zhang, Junjie Hao, Zhimeng Guo, Zhenhui Ji, Ji Luo, Cunguang Chen, and **Fang Yang**, Institute for Advanced Materials and Technology, University of Science and Technology Beijing, 30 Xueyuan Road, Haidian District, Beijing 100083, China; and **Alex A. Volinsky**, Department of Mechanical Engineering, University of South Florida, Tampa, FL 33620. Contact e-mails: haojunjie@ustb.edu.cn and volinsky@usf.edu.

heater assembly has to be modified to improve performance and reliability, which are governed by ceramics thermal conductivity, electrical resistivity and density (Ref 6). Improving thermal conductivity and density of standard alumina potting without too many additions and with low shrinkage is of great interest.

Usually, the heater assembly is formed centrifugally using a ceramic slurry, wire and the support cylinder, and then dried and sintered together. According to the wet forming theory, high solid-loaded alumina slurries with low viscosity are conducive to increase potting density. Theoretical (Ref 7-13) and experimental research reports (Ref 13-24) demonstrate that proper particle size distribution can significantly improve properties of the solid-phase slurry, improve particle accumulation and increase green body density. On the other hand, investigations of Heunisch (Ref 25) and Wang (Ref 23, 26) showed that slurries made with spherical particles exhibit lower viscosity with similar particle loading and green body, leading to higher green density than platelet-shaped particles and ground powder. Spherical powders allow easier particle rearrangement and pack more densely (Ref 25). In addition, Ferreira et al. (Ref 20, 27) and Taruta et al. (Ref 21) have shown for Al_2O_3 that it is possible to obtain high-density slip cast bodies by using bimodal powder size distribution (PSD), in which fine and coarse powders are combined with an appropriate proportion and size ratio. In particular, Tari et al. (Ref 27) demonstrated obtaining high solid-loaded alumina slurries with 70 vol.% and different PSD.

In the present work, both different particle size distribution and spherical particles are used to produce high solid-loaded alumina slurries with low viscosity, which has not been reported previously. The slurries were produced for centrifugal casting, and their rheological behavior was analyzed. Thermal conductivity and density of the standard alumina potting were investigated experimentally and correlated with microstructure.

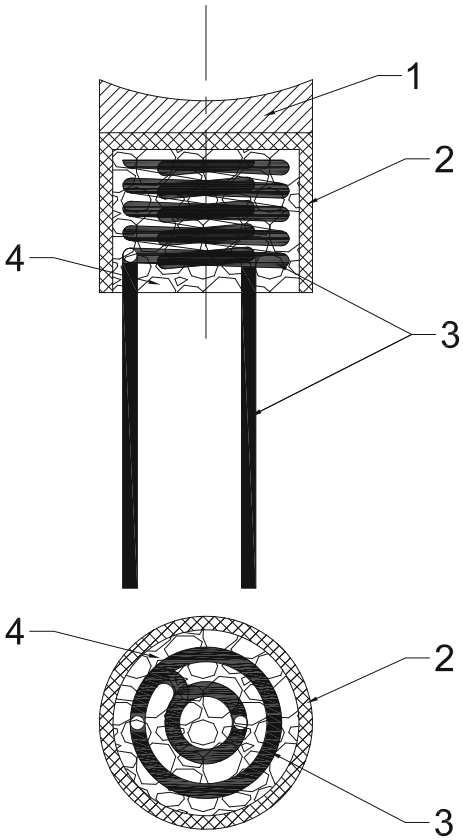

Fig. 1 Heater assembly geometry: 1—cathode, 2—support cylinder, 3—coiled filament wire, 4—alumina potting

2. Experimental Procedure

2.1 Powder Characterization

Spherical alumina powder (SAP) and irregular-shape alumina powder (IAP) with a different particle size (PS) and shape were used as starting materials of the slurries for the potting process. SEM morphology of the powders is shown in Fig. 2. The IAP powder contains irregularly shaped particles, while the SAP powder is spherical with almost 90% spheroidization. The IAP powder was obtained from Denka, Tokyo, Japan. In contrast, the particles for the SAP powder were prepared by the authors using plasma spheroidization in the RF thermal plasma reactor from the IAP powder. The particle size distribution and the specific surface area of all powders were determined by laser granulometry (Mastersizer 2000, Malvern Instruments, Worcestershire, UK) after powder dispersion by ultrasonic treatment and addition of ammonium citrate (Sinopharm Chemical Reagent Beijing Co., Ltd, China) as a dispersant. The particle shape was characterized by scanning electron microscopy (SUPRA 55, Carl Zeiss Company, Germany).

2.2 Slurry Preparation

From these powders, slurries with 60-70 vol.% solid content were prepared. Deionized water was used as a solvent and ammonium citrate (AC), or polycarboxylic acid (PC) was added as a dispersant. All dispersants are completely water-soluble and were provided by the manufacturers in the aqueous solution form. Then, the pH value of deionized water was adjusted to 10-11 by adding ammonia. Two kinds of alumina powders were blended in different proportions with the solvent. For complete deagglomeration of the powder particles, the slurries with solid content were milled in a ball mill for 12 h. Subsequently, the slurry was sieved through a 200-μm mesh screen and degassed to remove trapped gas bubbles before centrifugal casting.

Zeta potentials of dilute alumina slurries were measured using zeta potential analyzer (Zetasizer Nano ZS, Malvern, Worcestershire, UK). An aqueous suspension was used to measure the zeta potential with the solid concentration of about 0.02 wt.% using IAP powders. The dispersants were added based on the weight of the powder, and then, the pH was adjusted by HCl and NaOH solutions with corresponding pH values of 3 and 11. Rheological behavior was characterized using a rotational rheometer (MCR 300, Physica, Germany). The viscosity of the slurries was measured with continuous shear rate, γ, increasing from 0.1 to 100 s^{-1} at 20 °C.

2.3 Centrifugal Casting

Support cylinder and coiled filament wire were washed in acetone, followed by alcohol rinse and post-bake. First, the degassed slurry was poured into the support cylinder. Then, the wire was inserted into the slurry wrapped by the support cylinder. They were spun in an aluminum mold for 5 min at 2000 g centrifugal force in a centrifuge (Optima L-XP, Beckman, USA) equipped with swinging buckets. Meanwhile, for each set of parameters, centrifugal casting alumina potting

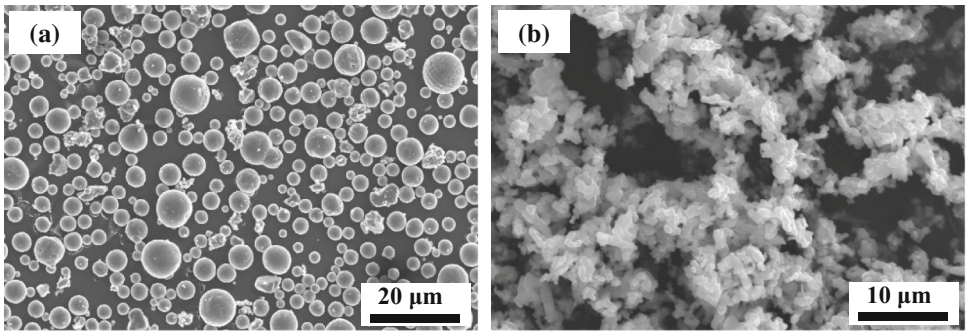

Fig. 2 Scanning electron micrographs of the two as-received alumina powders: (a) SAP; (b) IAP

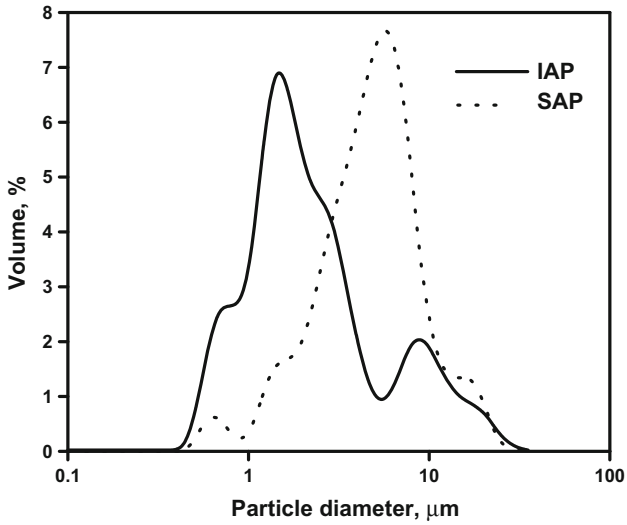

Fig. 3 Particle size distribution of the alumina powders

samples (ϕ12.5 mm × 20 mm) were made using a plastic centrifuge tube. For each sample, the weight and size were measured by means of precision scales and micrometer, respectively. The green density was calculated accordingly.

2.4 Samples Sintering

After drying, the heater assembly samples were fired in vacuum using the following temperature–time profile: the heating rate of 3 °C/min up to 200 °C, 5 °C/min to the maximum temperature of 1600 °C, 60 min dwell time, followed by the cooling rate of 5 °C/min under hydrogen atmosphere. Thermal diffusivity was determined using the laser pulse method by the thermal diffusivity system (LFA447 Nanoflash, Germany) of the samples (12.5 mm diameter and 2.5 mm thickness) with conductive Au sputter coating on both sides in the 200-800 °C temperature range. For the sintered samples, density and size were determined again. The shrinkage was calculated using the size values in green and sintered states.

3. Results and Discussion

Medium particle size d_{50} of the SAP spherical powder was 4.8 μm, and that of the IAP was 1.8 μm. Particle size distribution obtained by laser granulometry is shown in Fig. 3. The distribution of the two kinds of powders has two peaks with a wide intersection region. Specific surface area of the powders was obtained from the data in Table 1.

Table 1 Medium particle size d_{50} and specific surface area of the Al_2O_3 powders

Powder	d_{50}, μm	Specific surface area, m^2/g
IAP	1.8	1.21
SAP	4.8	0.57

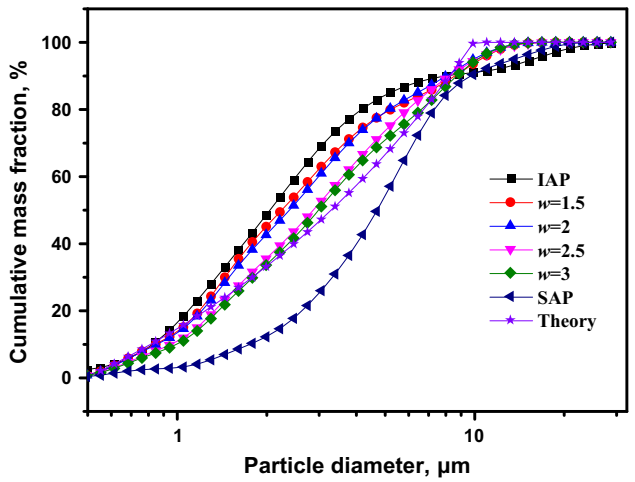

Fig. 4 Particle size distribution of mixed powders and calculated results by the Dinger packing model, w = m(SAP)/m(IAP)

3.1 Particle Size Distribution Analysis

Two kinds of alumina powders were blended in different proportions to study particles packing. This introduces a variable w, which is the mass ratio of SAP to IAP. According to the continuous particle distribution model proposed by Funk and Dinger (Ref 9-12, 24), to maximize powder packing efficiency, particle distribution needs to satisfy Eq 1:

$$w_{particle} = \frac{d^n - d_{min}^n}{d_{max}^n - d_{min}^n} \quad \text{(Eq 1)}$$

where d, $d_{\min}$ and $d_{\max}$ denote the particle size, minimum and maximum particle sizes, respectively, and w_{particle} is the cumulative mass fraction of powders with size less than d.

Table 2 Potting materials' properties before and after sintering

w	ρ_g, g/cm^3	ρ'_g, %	ρ_s, g/cm^3	ρ'_s, %	ε, %		α, mm^2/s	k, W m^{-1} K^{-1}
					Top	Bottom		
0:1	2.19	54.75	3.1	77.5	12.25	11.5	6.62	14.78
1.5:1	2.82	70.5	3.38	84.5	13.8	5.5	8.24	20.05
2:1	2.79	69.75	3.31	82.75	5.9	5.9	8.66	20.64
3:1	2.81	70.25	3.47	86.75	6.3	5.5	8.86	22.14
4:1	2.84	71	3.16	79	6.3	6.7	8.47	19.27
1:0	2.4	60	2.83	70.75	4.75	4.75	6.5	13.99

ρ_g, ρ'_g, ρ_s and ρ'_s represent the green body density, green body relative density, sintered density and sintered relative density, respectively.

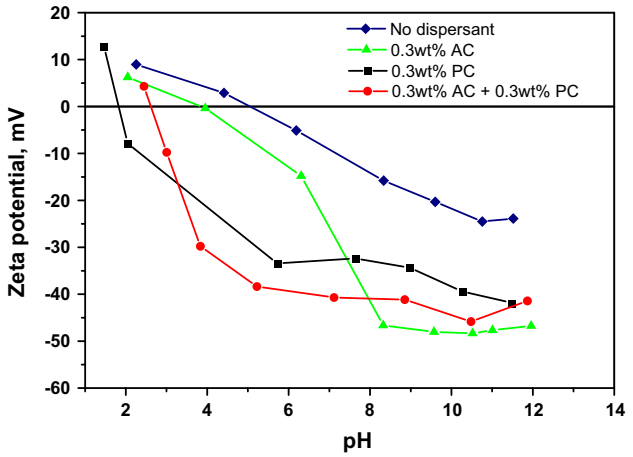

Fig. 5 Dispersants effects (wt.% of Al_2O_3 powders) on the zeta potential

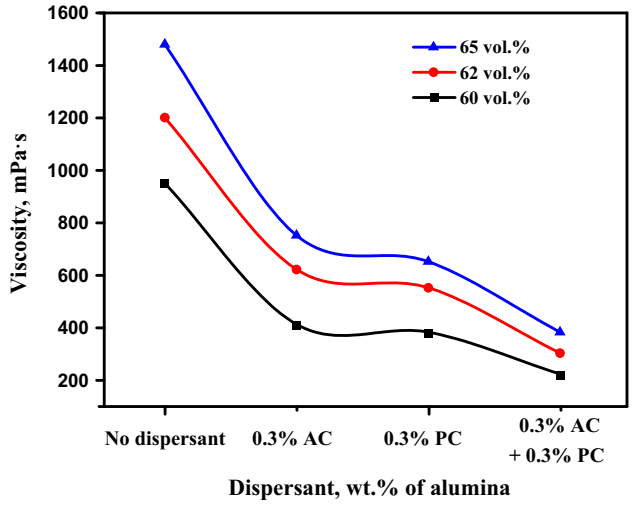

Fig. 6 The viscosity of the Al_2O_3 slurry with different dispersants (wt.% of Al_2O_3); w = 3; shear rate = 100 s^{-1}

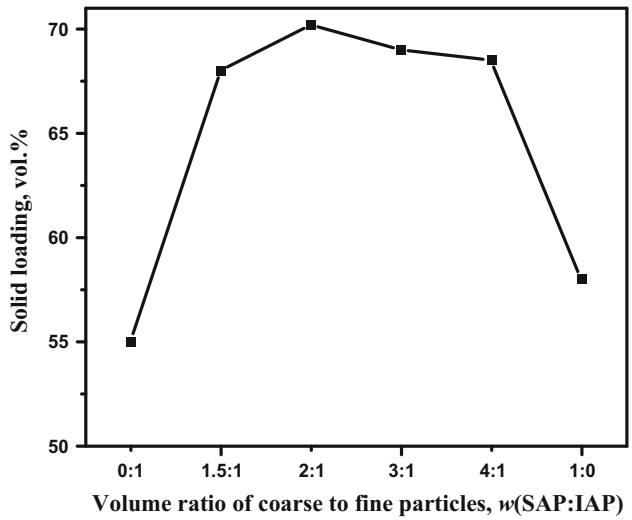

Fig. 7 The relationship between the maximum of solid loading and the volume ratio of the two as-received powders

The distribution modulus n is 0.37, given by the Dinger model for the three-dimensional conditions. The minimum particle size was 0.5 μm, and the maximum particle size was 12 μm in the mixture of IAP and SAP powders. The calculation results are shown in Fig. 4, where the mass ratio of SAP to IAP, w, was 3-4, and particle size distribution of the mixture is close to theoretical predictions. Table 2 lists potting materials' properties before and after sintering.

3.2 Dispersants Effects on Slurries Properties

According to the extended Derjaguin, Landau, Verwey and Overbeek (DLVO) theory, the properties of the suspensions are not only controlled by PS and PSD (Ref 27), particle shape (Ref 23), solid loading (Ref 28), but also by the interaction forces between suspended particles. Ceramic powders tend to agglomerate due to the attractive inter-particle van der Waals forces (Ref 28). Appropriate dispersants alter the powder surface properties so that the repulsive forces become higher than the attractive forces and the particles can remain separated in suspension. The repulsive forces consist of either electrostatic repulsion resulting from the overlapping of electrical double layers or steric hindrance resulting from absorption of large molecules (Ref 29). Dispersants that are functioning via both electrostatic and steric mechanisms are called poly-electrolytes, which usually consist of a hydrocarbon chain and a polar ionic part (COO^-, SO_3^-) (Ref 30-32). Dispersant addition can dramatically reduce the viscosity of slurries with very high solids content, and thus, ceramic industry has a constant demand for effective dispersants (Ref 33). Zeta potential measurements are used for preliminary screening among various dispersants, such as AC and PC. An AC molecule

has three polar ionic parts, COO^-, which have small molecular weight and can observably increase electrostatic repulsion of particles. However, PC will apparently enhance steric hindrance related to long carbon chain and polar ionic part with 5000-10,000 molecular weight. Figure 5 shows the effects of dispersants (wt.% of Al_2O_3 powders) on the zeta potential. Figure 6 shows the change of viscosity of the Al_2O_3 slurry with different dispersants (wt.% of Al_2O_3 powders).

3.3 Slurries Rheological Properties

Slurries with the highest solid concentration were prepared by adding powders continuously until the slurries could not flow. The relationship between the maximum of solid loading and the volume ratio of the two as-received powders is shown in Fig. 7. With higher volume ratio of the IAP powder, the solid loading first increases and then decreases. It is obvious that the solid loadings of slurries using only one kind of powder, either IAP or SAP, were far less than the ones using the mixture of the two powders, corresponding to 55 and 58 vol.%. The solid loading reached the 69.3-70.2 vol.% maximum when the two powders were present in proportion with the proper amount of dispersants. The solid loading was 68 and 68.5 vol.% when w was 1.5 and 4, respectively. Figure 7 shows that bimodal PSDs can maximize the solid loading of the slurries, which is consistent with the previous research. Figure 4 and 5 show that the ratio of the two as-received powders (w = 2-3), which achieve maximum solid loading, is very close to the theoretical value (w = 3-4) calculated by the Dinger model. According to the Dinger model, the finer particles can substitute the space occupied by the solvent between the particles in slurries, and thus, the amount of solvent decreased and the solid loading increased. Meanwhile, the replaced solvent was free in the slurry, improving its rheological behavior.

The heater assembly has complex geometry, and its external diameter ranges from 3 to 15 mm. Therefore, slurry excellent rheological properties are essential for the slurry to fully fill the internal space of the heater assembly. First, when the degassed slurry was poured into the support cylinder, it flowed and filled the space at a slow rate. Then, the heater assembly was spun in a centrifuge. The effects of the PSD on the equilibrium viscosity and the shear stress of the slurries with the constant solid loading of 65 vol.% are shown in Fig. 8. The slurries in different proportions (w = 1.5-3) showed pseudoplastic, plastic and dilatant fluid behavior under different shear rate ($\gamma < 1\ s^{-1}$; $1\ s^{-1} < \gamma < 20\ s^{-1}$; $\gamma > 20\ s^{-1}$), respectively.

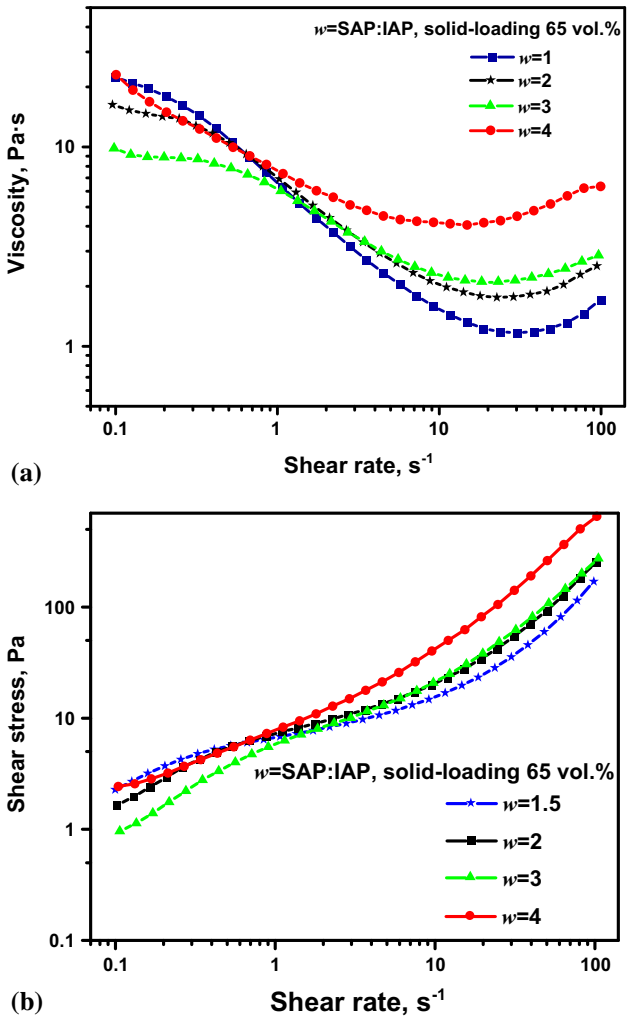

Fig. 8 Rheological curves of mixed suspensions: (a) viscosity, (b) shear stress

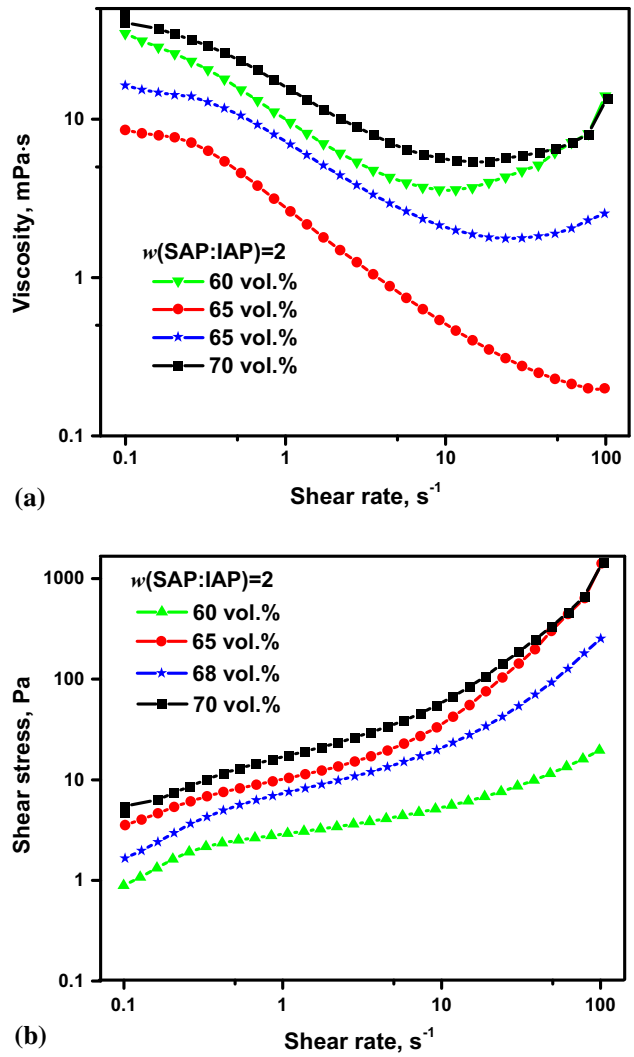

Fig. 9 Rheological curves of the slurries with different solid loading and w = 2: (a) viscosity, (b) shear stress

It is the Bingham fluid flow when the shear rate is lower than 10 s^{-1}, while rheological characteristics of the slurry (w = 4) exhibited shear thickening at the shear rate higher than 10 s^{-1}. These results illustrated that the four slurries showed rheological behavior, which can be depicted by the Bingham model. It can be seen that the slurries containing high proportions of the spherical and coarser SAP alumina powder show lower viscosity and shear stress under high shear rate, while the slurries obtained the lowest critical shear stress and initial viscosity when w = 3 under low shear rate with 65 vol.% solid loading.

The equilibrium viscosity and the shear rate gradually increased as the solid loading increased when w = 2, as shown in Fig. 9. The slurries showed pseudoplastic, plastic and dilatant fluid behavior with increasing shear rate when the solid loading was higher than 60 vol.%, while the 60 vol.% slurry is the Bingham fluid. Although the equilibrium viscosity slurry (70 vol.%) exhibited shear thickening under high shear rate, the slurries always had a flat surface at rest.

3.4 Sintering Behavior and Thermal Conductivity

Figure 10 shows typical fracture surfaces of Al_2O_3 potting material as green body and sintered at 1600 °C for 2 h. The alumina powders were tightly packed, and the IAP and SAP powders were well blended together in the green body. The spherical powders were closely compacted with each other, while the finer IAP powders fully filled the space between the spherical powders. Figure 10(b) depicts representative SEM micrographs of Al_2O_3 potting material sintered at 1600 °C. After sintering, new sintering necks were formed, and porosity decreased at the same time. The Al_2O_3 potting material microstructure is significantly different in terms of alumina particle morphology before and after sintering. The spherical powders no longer exhibit pronounced spherical shape. Furthermore, the IAP and SAP powders have changed from close packing to sintering densification. The apparent sintering necks were formed, greatly helping sintering densification and improving the thermal conductivity. Several transgranular fractures were observed, indicating that the Al_2O_3 potting material prepared with mixed powders was well sintered and had adequate strength.

Results are summarized in Table 2, where the sintering properties and thermal conductivity are listed. Figure 11 depicts the relative density change with increasing volume ratio of the spherical powder. The green body obtains the higher relative density of 70% with mixed powders than using only one kind of powder. However, there is no obvious difference between the different ratios of the two powders. The sintered relative density reaches 86.75% maximum, while the spherical powder is three times denser than the fine powder.

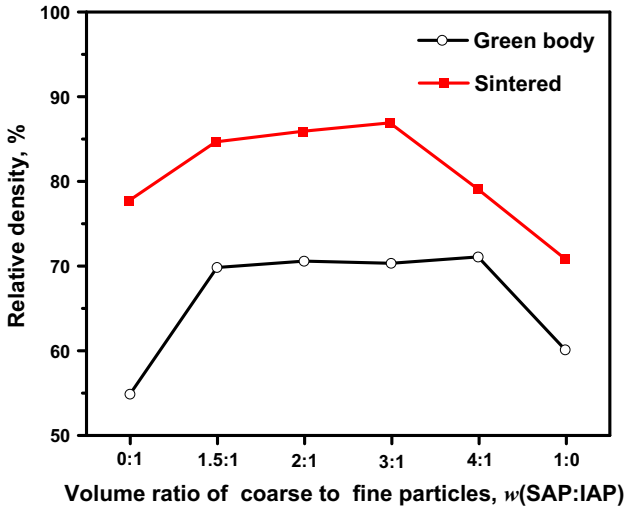

Fig. 11 The relationship between the relative density and the volume ratio of the two as-received powders

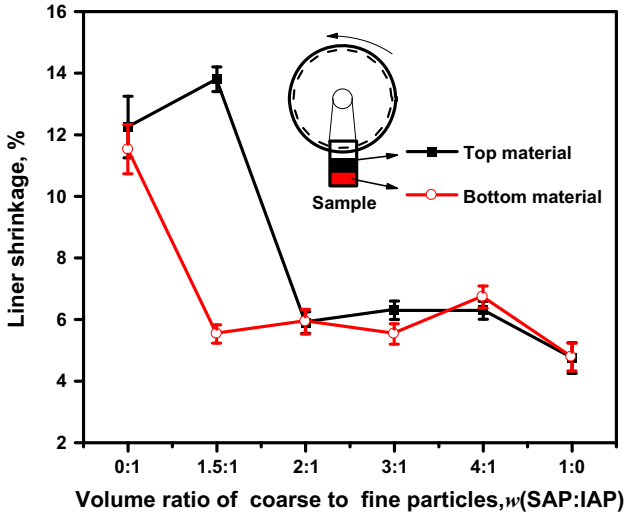

Fig. 12 The relationship between the liner shrinkage and the volume ratio of the two as-received powders

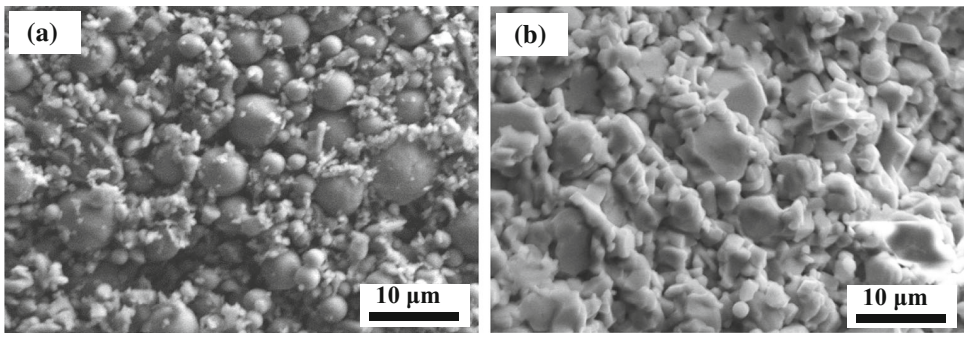

Fig. 10 Fracture surfaces of the Al_2O_3 potting material: (a) green body, (b) sintered at 1600 °C for 2 h

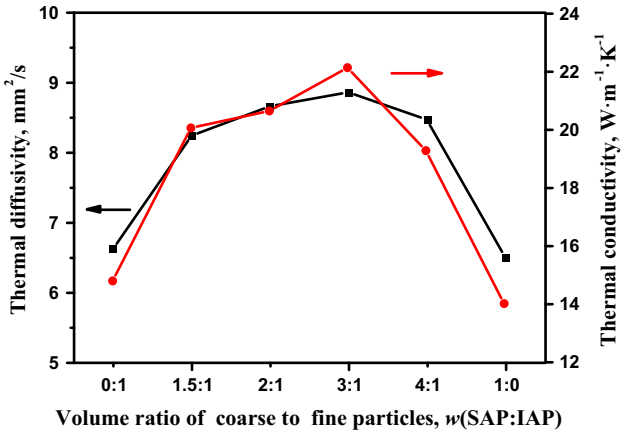

Fig. 13 Thermal diffusivity and thermal conductivity dependence on the volume ratio of the two as-received powders

Figure 12 shows the linear shrinkage behavior of the two kinds of powder with different ratios. After a lot of tests, some obvious cracks can be observed on the top or bottom of sintered samples with $w = 1.5$, 4 and only spherical powder. The finer the IAP powder, the larger the linear shrinkage, ε, because the finer powder is greatly conducive to sintering densification of the mixed powders. Since excessive IAP powders gather together on the top after centrifuging, cracks in the $w = 1.5$ samples appeared due to high shrinkage stress and large liner shrinkage difference between the top and bottom materials in Fig. 12. For $w = 4$ and pure spherical powder, excess SAP powders and lack of IAP powders cannot form enough effective sintering necks. Stress concentration due to sintering shrinkage leads to cracks initiation. When $w = 2$ and 3, the potting ratio is similar to the ideal material with high density with low shrinkage, and a small shrinkage difference between upper and lower materials.

Figure 13 shows that the thermal diffusivity, α, and thermal conductivity, k, first increased and then decreased as the ratio of coarser spherical powder increased. The thermal diffusivity and thermal conductivity both reach a maximum of 8.86 mm^2/s and 22.14 W/(m K), respectively, when $w = 3$. The potting material was prepared by centrifugal casting, pressureless sintering and without any sintering aids, and its thermal conductivity is obviously higher than previously reported (Ref 1-3, 5).

Since potting material relative density is smaller than 90%, it can be considered porous. It is generally known that the thermal conductivity of porous materials does not only depend on the solid component and porosity but also materials structure (Ref 34). Five basic structural models, including the series and parallel models (Ref 35), the Maxwell–Eucken model (Ref 36), and the effective medium theory (EMT) equation (Ref 37), were established to simulate the thermal conductivity of porous materials. In principle, although these modified models have been widely used, the data must accord with the series and parallel models with a suitable value of ξ (Ref 38). We can use a mixed relation as an empirical equation of the thermal conductivity of porous materials as:

$$k_p^{\xi} = k_c^{\xi}(1-\psi) + k_a^{\xi} \cdot \psi \qquad \text{(Eq 2)}$$

where k is the thermal conductivity, ψ is the porosity of the potting material, and ξ is the weight parameter. The subscripts p, c and a stand for the potting, ceramics and air pores, respectively. In this equation, the variable ψ changes from 0 to

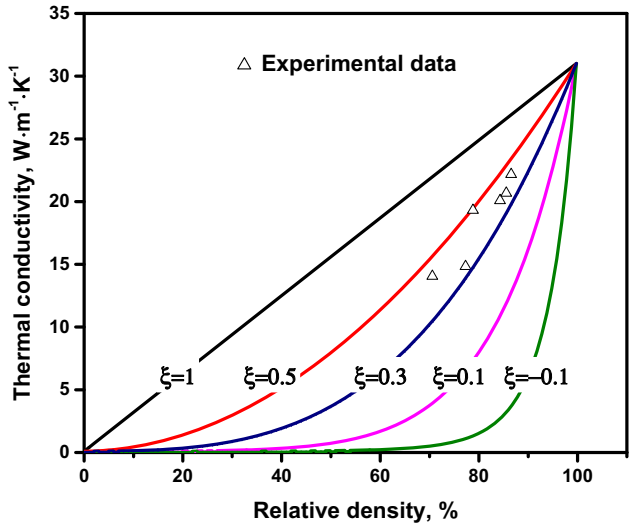

Fig. 14 Potting material thermal conductivity. The series and parallel models plotted with the experimental data

99.9% and k_a and k_c are calculated as 0.026 W/(m K) (Ref 38, 39) and 31 W/(m K), respectively. The weight parameter ξ ranges from -1 to 1. In fact, the ξ value reflects the factors including properties of the solid components, porosity and the structure of the materials. When the parameter $\xi = 1$, the solid is continuous, and the mechanism is the same as the parallel model:

$$k_p = k_c \cdot (1-\psi) + k_a \cdot \psi \qquad \text{(Eq 3)}$$

In contrast, when $\xi = -1$, the pores are continuous, and this situation is identical to the series model:

$$k_p = \frac{1}{\frac{1-\psi}{k_c} + \frac{\psi}{k_a}} \qquad \text{(Eq 4)}$$

Comparison of potting thermal conductivity values calculated using Eq 2 and experimental data with different relative density and ξ values is presented in Fig. 14. The experimental data values are distributed between the two curves $\xi = 0.3$ and $\xi = 0.5$. The series and parallel models were used to calculate the thermal conductivity and showed good agreement with experimental data.

4. Conclusions

In this work, alumina potting material with low linear shrinkage and high thermal conductivity was made for fast warm-up traveling-wave tube cathodes assembly. In this experiment, two types of alumina powders with different morphology and size were used to prepare high solid-loaded slurries as high as 70 vol.% when $w = 2$. Dispersants and milling were applied to deagglomerate alumina powders. The rheological behavior was analyzed. Fabrication of green body with relative density above 70% has been demonstrated from their slurries using centrifugal casting. The sintered relative density reached 86.75% maximum, the linear shrinkage reached 5.5% minimum, and the thermal conductivity reached 22.14 W/(m K) maximum. The potting material thermal conductivity agreed well with the series and parallel models when the weight parameter ξ was between 0.3 and 0.5.

Acknowledgments

This work was supported by the State Key Lab of Advanced Metals and Materials (Grant No. 2018-Z06). AV acknowledges support from the National Science Foundation (IRES 1358088).

References

1. D.S. Orlowska, Fast warm cathode—practical fielded design, in *National Vacuum Electronics Conference* (Surrey Ion Beam Centre, 2007)
2. K.S. Pal, S. Ghosh, N. Dandapat, S. Datta, D. Basu, and R.S. Raju, Development of Suitable Potting Material for Dispenser Cathodes of a High Power Microwave Tube, *Mater. Sci. Eng. B*, 2012, **177**(2), p 228–232
3. P. Swartzentruber, M. Collier, R. Dewees, and W. Epperson, Alternative ceramic potting materials for dispenser cathodes, in *Vacuum Electronics Conference* (2012), pp. 483–484
4. C.W. Park and D.Y. Yoon, Effect of SiO_2, CaO_2 and MgO Addition on the Grain Growth of Alumina, *J. Am. Ceram. Soc.*, 2000, **83**(10), p 2605–2609
5. L. Wolverton, J.O. Tarter, R.E. Eitel, and M. Weisenberger, P1–33: Thermal properties of alumina cathode heater potting materials, in *Vacuum Electronics Conference (IVEC)*, (2010), p. 165
6. L.R. Falce, Dispenser cathodes: The current state of the technology, in *International Electron Devices Meeting* (1983), pp. 448–451
7. G.L. Messing and G.Y. Onoda, Inhomogeneity-Packing Density Relations in Binary Powders—Experimental Studies, *J. Am. Ceram. Soc.*, 1978, **61**(7–8), p 363–366
8. J.A. Dodds, The Porosity and Contact Points in Multicomponent Random Sphere Packings Calculated by a Simple Statistical Geometric Model, *J. Colloid Interface Sci.*, 1980, **77**(2), p 317–327
9. J. Funk and D. Dinger, Packing of Discrete Versus Continuous Particle Size Distributions, *Interceramic*, 1992, **41**(5), p 332–334
10. J. Funk and D. Dinger, Fundamentals of Particle Packing, Monodisperse Spheres, *Interceramic*, 1992, **41**(1), p 10–14
11. J. Funk and D. Dinger, Review of Packing in Polydisperse Particle Systems, *Interceramic*, 1992, **41**(2), p 95–97
12. J. Funk and D. Dinger, Computer Modelling of Particle Packing Phenomena, *Interceramic*, 1993, **42**(3), p 150–153
13. J. Zheng, W.B. Carlson, and J.S. Reed, The Packing Density of Binary Powder Mixtures, *J. Eur. Ceram. Soc.*, 1995, **15**(5), p 479–483
14. K.R. McGeary, Mechanical Packing of Spherical Particles, *J. Am. Ceram. Soc.*, 1961, **44**(10), p 513–522
15. A.B. Yu, N. Standish, and A. Mclean, Porosity Calculation of Binary Mixtures of Nonspherical Particles, *J. Am. Ceram. Soc.*, 1993, **76**(11), p 2813–2816
16. P.A. Smith and R.A. Haber, Effect of Particle Packing on the Filtration and Rheology Behavior of Extended Size Distribution Alumina Suspensions, *J. Am. Ceram. Soc.*, 1995, **78**(7), p 1737–1744
17. S. Taruta, N. Takusagawa, K. Okada, N. Otsuka, S. Taruta, N. Takusagawa, K. Okada, and N. Otsuka, Slip Casting of Alumina Powder Mixtures with Bimodal Size Distribution, *J. Ceram. Soc. Jpn.*, 1996, **104**(1209), p 447–450
18. G.T. Igrave, J.M.F. Ferreira, A.T. Fonseca, and O. Lyckfeldt, Influence of Particle Size Distribution on Colloidal Processing of Alumina, *J. Eur. Ceram. Soc.*, 1998, **18**(3), p 249–253
19. J.M.F. Ferreira and H.M.M. Diz, Pressure Slip Casting of Bimodal Silicon Carbide Powder Suspensions, *Ceram. Int.*, 1999, **25**(6), p 491–495
20. G. Tari, J.M.F. Ferreira, and A.T. Fonseca, Influence of Particle Size and Particle Size Distribution On Drying-Shrinkage Behaviour of Alumina Slip Cast Bodies, *Ceram. Int.*, 1999, **25**(6), p 577–580
21. S. Taruta, Y. Sakurai, N. Takusagawa, K. Okada, and N. Otsuka, Slip Casting of Alumina Powder Mixtures with Bimodal Size Distribution: Influence of Particle Size Difference Between Fine and Coarse Powders on Packing and Consolidation Process, *J. Ceram. Soc. Jpn.*, 2000, **108**, p 254–260
22. J.U. Chenhui, W. Yanmin, Y.E. Jiandong, L.I. Xinheng, W. Yanmin, Y.E. Jiandong, and L.I. Xinheng, Effect of Particle Size Distribution on the Rheological Behavior of Dense Alumina Suspensions, *J. Chin. Ceram. Soc.*, 2006, **34**(8), p 985–991 (in Chinese)
23. W. Qi, C. Wei, G. Yiyao, and X. Zhipeng, Preparation and Sintering Properties of Alumina Slurries with High Solid Loading, *Rare Metal Mat. Eng.*, 2013, **42**(S1), p 400–403 (in Chinese)
24. Y. Sun, S. Shimai, X. Peng, M. Dong, H. Kamiya, and S. Wang, A Method for Gelcasting High-Strength Alumina Ceramics with Low Shrinkage, *J. Mater. Res.*, 2014, **29**(02), p 247–251
25. A. Heunisch, A. Dellert, and A. Roosen, Effect of Powder, Binder and Process Parameters on Anisotropic Shrinkage in Tape Cast Ceramic Products, *J. Eur. Ceram. Soc.*, 2010, **30**(16), p 3397–3406
26. Z. Fu, P. Polfer, T. Kraft, and A. Roosen, Correlation Between Anisotropic Green Microstructure of Spherical-Shaped Alumina Particles and Their Shrinkage Behavior, *J. Am. Ceram. Soc.*, 2015, **98**(11), p 3438–3444
27. G. Tarì, J.M.F. Ferreira, A.T. Fonseca, and O. Lyckfeldt, Influence of Particle Size Distribution on Colloidal Processing of Alumina, *J. Eur. Ceram. Soc.*, 1998, **18**(3), p 249–253
28. A. Tsetsekou, C. Agrafiotis, and A. Milias, Optimization of the Rheological Properties of Alumina Slurries for Ceramic Processing Applications Part I: Slip-Casting, *J. Eur. Ceram. Soc.*, 2001, **21**(3), p 363–373
29. R.G. Horn, Surface Forces and Their Action in Ceramic Materials, *J. Am. Ceram. Soc.*, 1990, **73**(5), p 1117–1135
30. C.J. Brinker and G.W. Scherer, *Sol–Gel Science*, Academic press, Boston, 1990
31. S.J. Schneider, *Engineered Materials Handbook*, ASM International, Geauga, 1991
32. E. Carlström, *Surface and Colloid Chemistry in Ceramics: An Overview*, Marcel Dekker, New York, 1994
33. R. Moreno, The Role of Slip Additives in Tape Casting Technology 2. Binders and Plasticizers, *Am. Ceram. Soc. Bull.*, 1992, **71**(11), p 1647
34. L. Miettinen, P. Kekäläinen, T. Turpeinen, J. Hyväluoma, J. Merikoski, and J. Timonen, Dependence of Thermal Conductivity on Structural Parameters in Porous Samples, *AIP Adv.*, 2012, **2**(1), p 2150–2240
35. A.G. Leach, The Thermal Conductivity of Foams. I. Models for Heat Conduction, *J. Phys. D Appl. Phys.*, 1999, **26**(5), p 733
36. Z. Hashin and S. Shtrikman, A Variational Approach to the THEory of The Effective Magnetic Permeability of Multiphase Materials, *J. Appl. Phys.*, 1962, **33**(10), p 3125–3131
37. R. Landauer, The Electrical Resistance of Binary Metallic Mixtures, *J. Appl. Phys.*, 1952, **23**(7), p 779–784
38. L. Gong, Y. Wang, X. Cheng, R. Zhang, and H. Zhang, A Novel Effective Medium Theory for Modelling the Thermal Conductivity of Porous Materials, *Int. J. Heat Mass Transfer*, 2014, **68**(1), p 295–298
39. H. Shenker, J.I. Lauritzen, R.J. Corruccini, and S.T. Lonberger, Reference Tables for Thermocouples, 564 (1955)